

Behavior and Performance of Reinforced Concrete Columns Subjected to Accelerated Corrosion

Asif Hameed¹, Muhammad Faheem Ud Din Afzal^{2,*}, Ali Javed², Ali Murtaza Rasool^{3,4,*},
Mohsin Usman Qureshi⁵, Armin B. Mehrabi² and Imran Ashraf¹

- ¹ Civil Engineering Department, University of Engineering and Technology, Lahore 54000, Pakistan; asifhameed@uet.edu.pk (A.H.); imran.ashrafuet@yahoo.com (I.A.)
- ² Department of Civil and Environmental Engineering, Florida International University, Miami, FL 33174, USA; ajave010@fiu.edu (A.J.); amehrabi@fiu.edu (A.B.M.)
- ³ Diamer Basha Dam Consultant Group (DBCG)—National Engineering Services Pakistan (NESPAK), Lahore 54000, Pakistan
- ⁴ Visiting Faculty, University of Central Punjab (UCP), Lahore 54000, Pakistan
- ⁵ Faculty of Engineering, Sohar University, P.O. Box. 44, Sohar 311, Oman; mqureshi@su.edu.om
- * Correspondence: mafza001@fiu.edu (M.F.U.D.A.); ali.murtaza@nespak.com.pk (A.M.R.)

Abstract: Steel reinforcement corrosion in concrete structures such as bridges, industrial plants, marine structures, and coastal buildings is a growing concern due to its impact on cost, safety, and serviceability. Corrosion leads to spalling, cracking, and reduced reinforcement diameter, which can compromise structural integrity. This study examines the behavior of concrete columns with corroded reinforcement in two phases. In the first phase, 72 columns of 150 × 150 mm cross-sectional dimensions and 300 mm length were cast and subjected to an accelerated corrosion technique. The study examined variables such as concrete cover, concrete strength, and corrosion exposure. The second phase involved studying the axial behavior of corroded columns concerning the effect of column length. Column specimens of 150 × 150 mm cross-sectional dimensions and lengths of 500 mm, 700 mm, and 900 mm were cast, corroded, and tested under axial compressive load. The study revealed that a 30 mm concrete cover offers 10% more protection against corrosion than a 20 mm cover. Continuous exposure to a corrosive environment reduces the load-carrying capacity by 50%, while columns with 28 MPa concrete strength can carry 4% more load. Longer columns are more susceptible to corrosion, leading to a significant reduction in load-carrying capacity and concrete cover damage. Therefore, maintaining adequate concrete cover, strength, and regular inspections are essential to address steel reinforcement corrosion and preserve structural integrity.

Keywords: reinforced concrete columns; corroded rebars; corrosion exposure; axial performance; concrete cover



Citation: Hameed, A.; Afzal, M.F.U.D.; Javed, A.; Rasool, A.M.; Qureshi, M.U.; Mehrabi, A.B.; Ashraf, I. Behavior and Performance of Reinforced Concrete Columns Subjected to Accelerated Corrosion. *Metals* **2023**, *13*, 930. <https://doi.org/10.3390/met13050930>

Academic Editor: Yanxin Qiao

Received: 9 April 2023
Revised: 4 May 2023
Accepted: 8 May 2023
Published: 10 May 2023



Copyright: © 2023 by the authors. Licensee MDPI, Basel, Switzerland. This article is an open access article distributed under the terms and conditions of the Creative Commons Attribution (CC BY) license (<https://creativecommons.org/licenses/by/4.0/>).

1. Introduction

Reinforced concrete (RC) is a versatile construction material used globally for its durability [1], premature failures such as the Lowe's Motor Speedway Bridge collapse in North Carolina in 2000 raised concerns [2]. Even with the ever-increasing development of sustainable materials [3–6] and use of alternative reinforcement [7], corrosion remains a worldwide issue causing millions of dollars in losses annually [8] and is a major contributor to the degradation of reinforced concrete structures. Furthermore, failures in reinforced structures can also be attributed to defects that are not related to engineering [9,10]. Deterioration due to the aging of reinforced concrete members necessitate the repair of concrete structures [11]. Accurate evaluations of the aerodynamic characteristics of these structures are necessary to ensure their stability and safety, given their adaptable nature [12–15]. Steel embedded within concrete corrodes when the external environment alters [16] the composition of the pore solution present in the concrete, leading to the destruction of the passive oxide film

formed on the steel. Corrosion results in a loss of steel area provided during the design phase, leading to a reduction in the load carrying capacity of the sections. As a counter measure, numerous researchers adopted non-destructive techniques to detect damage to reinforcement that is related to corrosion [17]. The rate of corrosion is affected by factors such as the environment, cover thickness, concrete alkalinity and permeability, steel type, chloride environment, and cracks. Considering the growing use of additive manufacturing in the construction sector, it is crucial to comprehend the consequences of corrosion [18].

Chloride-induced corrosion of steel rebar is a common cause of concrete deterioration, resulting in physical degradation of reinforced concrete elements, including cracking of concrete cover, reduction in bond strength between concrete and steel, and loss of cross-sectional area of reinforcing steel due to rust formation. These combined effects compromise the load-carrying capacity and safety of structural elements such as beams, slabs, and columns especially in marine and chloride-rich environments [19]. The corrosion of beams and slabs usually causes their collapse, while the corrosion of columns can lead to the entire structure collapsing. While researchers studied the flexural behavior of corroded beams and slabs and seismic performance of corroded columns [20–23], less attention was given to the axial behavior of corroded columns. Therefore, significant experimental work was carried out to investigate the behavior of reinforced concrete columns affected by steel bar corrosion.

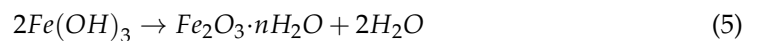
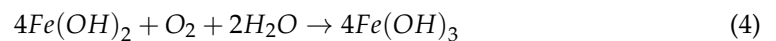
Uomoto [24] discovered that corroded reinforced concrete columns and beams showed reduced load-carrying capacity due to loss of reinforcement diameter and concrete cover spalling. Increasing current density did not always result in a linear decrease in load carrying capacity. After a certain value of current density, the concrete core carried the load primarily. The two least corroded columns had residual load carrying capacities of 88% and 98% of control samples, while the other six ranged from 77% to 84%. Rodriguez [25] studied the impact of accelerated corrosion on 24 concrete columns, grouped by reinforcement samples and exposed to a current density of 0.1 mA/cm². Both reinforcement diameter loss and spalling of concrete cover contributed to reduced load-carrying capacity. Corrosion decreased axial load capacity to a point beyond which further corrosion had no effect. Loss of gross area converted columns from stocky to slender, increasing effective length. Azad [26] studied the behavior of 48 concrete samples under eccentric axial loading, with 36 corroded. Load capacity reduction was due to reinforcement area loss and bond strength reduction from corrosion. Higher I_{CORRT} values led to greater strength reduction. Residual strength under combined loading was affected by corrosion-induced damaging effects beyond reinforcement area loss.

This study aims to investigate the behavior of reinforced concrete (RC) columns when subjected to concentric axial loads after undergoing accelerated corrosion. Furthermore, the study aims to examine the effect of accelerated corrosion duration on the behavior of RC columns. In addition, the study analyzes the impact of concrete cover on the resistance of reinforced concrete structures against corrosion. The study utilizes different concrete strengths to determine the effect of this parameter on the resistance to corrosion of reinforced concrete structures.

2. Corrosion Mechanism

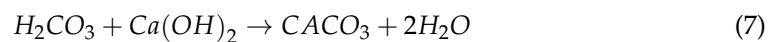
Steel reinforcement in concrete corrodes due to an electrochemical reaction, with the solution in the concrete acting as an electrolyte and the reinforcement as an electrical conductor. Corrosion begins with electron release at the anode, followed by their reaction with oxygen and water to form hydroxyl ions at the cathode [27]. Water and oxygen accelerate the corrosion process, leading to reactions between hydroxyl and iron ions that corrode the reinforcement [28], as shown in Equations (3)–(5). The variable ‘ n ’ in Equation (5) depends on the presence of water and oxygen. Corrosion usually starts with a

puncture in the resistive layer or cover of the steel reinforcement in concrete, which can be caused by carbonation, chloride ion attacks, and freeze–thaw cycles [29].



2.1. Carbonation

Carbonation of concrete is the chemical reaction of portlandite, $Ca(OH)_2$, in the cement matrix with carbon dioxide (CO_2) gas leading to calcite ($CaCO_3$) [30]. The reaction between carbon dioxide and concrete produces carbonic acid (H_2CO_3), as shown in Equation (6). Carbonic acid then reacts with calcium hydroxides in the pore solution, producing calcium carbonate ($CaCO_3$), as shown in Equation (7). This lowers the pH value below 10 and disrupts the passive layer around steel reinforcement, leading to corrosion. Corrosion from carbonation is influenced by factors such as permeability, concrete quality, concrete cover, and surrounding carbon dioxide levels [31]. Carbonation can be monitored using a pH indicator such as phenolphthalein, which turns clear in carbonated regions and pink in un-carbonated regions when exposed to the concrete surface.



2.2. Chloride Ions Attack

Chloride-induced corrosion is a costly and challenging deterioration for concrete infrastructure. Sea water, accelerators, and chloride-polluted aggregates are major sources of chlorides in concrete. Sea salt spray, de-icing salts, and alternate wetting and drying of offshore structures also contribute to chloride presence. Unlike carbonation, chloride ion attack does not neutralize the passive layer. Chloride ions act as catalysts, remaining present and attacking the reinforcement surface [32]. Chloride ions disturb the passive layer surrounding embedded steel reinforcement, reacting with ferrous ions at the anode to form a soluble compound that oxidizes into insoluble iron hydroxide at the cathode, producing chloride ions. These ions can continue to react with iron ions [27]. Chloride ions permeate and accumulate on embedded steel reinforcement mainly through diffusion. Contributing factors to chloride ion attack include concrete cover, cracks, and water/cement ratio.

3. Effects of Corrosion

Corrosion can result in three types of damage to reinforced concrete structures, happening simultaneously: cracking in the concrete cover leading to spalling, loss of bond between the reinforcement and concrete, and reduction in cross-sectional area due to rust formation. These effects reduce the load-carrying capacity of the column or member, reduce ductility, and primarily affect the concrete cover's cracking and bond strength [33]. Details on these mechanisms are explained below.

3.1. Cracking

Cracking of concrete cover is a potential effect of embedded steel corrosion as rust product occupies more volume than the original reinforcement bars. Several researchers investigated the conditions under which corrosion of reinforcement occurs.

Andrade [34] studied the effects of accelerated corrosion on concrete samples. Changing cover and current density impacted cracking, but calculated section loss may be overestimated due to initial infiltration of corrosion products into concrete pores. Chernin [35] presented a new analytical model for predicting cover cracking in concrete structures caused by corrosion of reinforcing steel. The model considers the concrete as a thick-walled cylinder subjected to pressure from corrosion products, leading to the formation of radial cracks. Guzman [36] studied the deterioration of reinforced concrete structures exposed to marine environments and presented two models for analyzing corrosion-induced cracking. The models were incorporated into a finite element program and compared with experimental results, resulting in a step forward in evaluating the service life of these structures. Alonso [34] conducted experiments on 27 concrete samples and found that the cover to bar diameter ratio and corrosion rate were significant factors in the amount of corrosion required to cause cracking. A higher corrosion rate required more corrosion to induce cracking and larger corrosion products were necessary to generate larger crack widths. Bossio [37] proposed FEM and analytical models to evaluate stress development and crack propagation due to pitting or general corrosion. It was found that crack propagation depends mostly on the concrete cover, while oxide penetration increases slightly as the elastic modulus of concrete decreases. Cabrera [38] conducted research on slabs with different bar diameters and cover types. Accelerated corrosion caused cracks in the bottom face of some slabs, while crack width had a linear relationship with corrosion. Faraday's law was used to calculate the amount of corrosion. A relation between crack width and increasing corrosion is plotted in Figure 1.

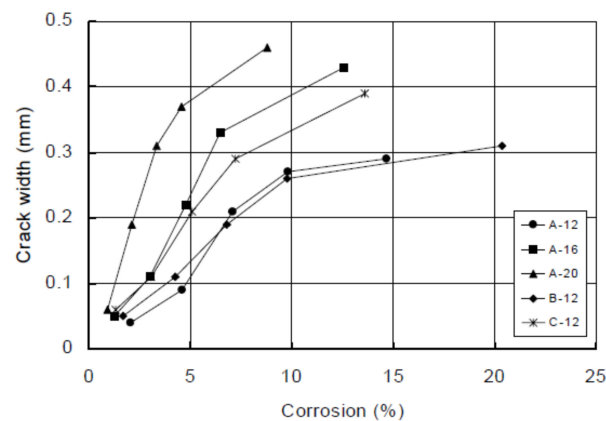


Figure 1. Relation of average crack width to corrosion, adapted with permission from Ref. [38]. 1996, Elsevier.

3.2. Bond Strength

Design codes and standards have a basic assumption that there is a perfect bond between the embedded reinforcement and concrete, as the strain in both is assumed to be equal. However, corrosion can negatively affect the bond strength of concrete elements.

Choi [39] found that corrosion of reinforcing bars in concrete structures reduces bond strength and stiffness, leading to deterioration and shortening of service life. Al-sulaimani [40] conducted experiments to investigate the bond strength of corroded specimens and found that pre-cracking and post-cracking stages are determined by the percentage of corrosion. Larger cover to rebar diameter ratios have a significant effect on bond strength, with larger amounts of corrosion required to produce the internal fine cracking necessary to reduce bond strength. Ma [41] observed that an increase in corrosion of a sample can significantly reduce bond strength once cracking has started. Clark and Saifullah [42]

conducted tests on plain and deformed reinforcement to study the influence of accelerated corrosion and concluded that the sharp decrease in bond strength before cracking is the main difference between the four stages of corrosion. Fang [43] showed that confinement can counteract bond loss for corroded steel bars, but substantial reduction in bond occurred when corrosion increased beyond 6%.

3.3. Mechanical Properties of Reinforcement

The corrosion of the reinforcement in the concrete can affect its mechanical properties due to the reduction in its cross-sectional area. Wang et al. [44] studied the effect of corrosion on reinforced concrete structures constructed using bimetallic steel bars. The accelerated corrosion led to a reduction in the tensile performance of the specimens. It also badly affected the low-cycle fatigue performance of the specimens. Hua et al. [45,46] investigated the mechanical properties of stainless steel rebars experimentally and numerically. They conducted tensile coupon test on the bimetallic bars which were corroded through accelerated electrochemical reactions. The results showed a clear yield plateau in the stress–strain curve of the bars. Francois et al. [47] checked the impact of corrosion on the mechanical properties of rebars in RC beams. The results showed a reduction in the ultimate elongation of all rebars. Apostolopoulos [48] investigated the influence of corrosion on mechanical properties of steel and found that corrosion is a major contributor in producing stress concentration points by creating pits and notches, which ultimately reduces ductility and tensile strength of the rebars.

4. Methodology

Corrosion in reinforced concrete structures can be reduced by improving quality of concrete and by providing thick cover around the rebars. It can also be reduced by using a low water/cement ratio. These preventive measures do not prove to be best in all environmental scenarios, especially where marine water or environment is in contact with the concrete structures. Several structures built according to modern codes and standards may be prone to the condition of reinforcement corrosion. To overcome this corrosion problem, there is a need to know more about corrosion process and its products. The experimental work conducted in this research consists of the following two phases.

4.1. Parametric Investigations

In parametric investigation, the concrete column specimens were cast and corroded in the lab. Parametric studies were performed previously for axially loaded piles [49] and also laterally loaded piles in multi layered soil [50]. Corrosion of embedded steel in concrete is a very slow process and it takes years to occur. Due to time constraints, the corrosion of the samples was performed artificially in the laboratory by passing the current through concrete samples. The original corrosion process is different than accelerated corrosion in the laboratory, and so, the study and effects of accelerated corrosion on concrete samples was required. In lieu of this, before commencing formal research, a series of preliminary tests to confirm the effectiveness of accelerated corrosion technique was performed on concrete columns. The following three parameters are considered to study this effect.

1. Concrete strength;
2. Cover to reinforcement diameter (c/D) ratio;
3. Level of corrosion in days.

Generally, the corrosion of reinforcement is carried out by impressed current technique. With help of this method, a significant corrosion of reinforcement can be achieved in limited time only. In the past, different researchers used impressed current technique to study the effect of reinforcement corrosion on concrete cover cracking, bond strength, and load bearing capacity of reinforced concrete members [51]. Some alternate methods were also suggested by various researchers. Ha [52] used an impressed voltage and microcell corrosion technique rather than impressed current technique to corrode reinforcement in concrete specimen. Yuan [53] created an artificial climate of high chlorides and humidity

level to simulate natural corrosion process to corrode reinforcement. Husain [54] evaluated performance of embedded reinforcement and its passivity breakdown by using accelerated AC impedance technique. C. Geng [55] devised a brand in technique in which chloride ions were diffused on to surface of embedded reinforcement that caused rapid corrosion of reinforcement. Auyenug [56] found that actual mass loss and theoretical mass loss due to impressed current technique were not the same due to factors such as the need of electrical energy to initiate corrosion, resistance of concrete, reinforcement composition, and due to electrical properties of minerals present within concrete. Based upon the results found by all cited technique, it can be summarized that impressed current technique is considered to be a very effective and reliable technique to induce corrosion in embedded reinforcement in the limited time available.

In impressed current technique, a DC source is supplied to embedded steel in concrete specimens which are placed in chloride solution. According to Care and Raharinaivo [57], concrete specimens should be immersed into solution containing chlorides rather than pure water because the immersed specimens obey the Faraday's law in case of chlorides, while in case of pure water, a complex phenomenon occurs during the process of accelerated corrosion method. After applying current for a specific duration, the weight loss of specimen is calculated by Faraday's law, as shown in Equation (8). Similarly, the percentage of actual amount of steel lost can be accessed by gravimetric test conducted on obtained reinforcement after crushing of concrete samples.

$$\Delta\omega = \frac{tAI}{FZ} \quad (8)$$

where $\Delta\omega$ is metal loss due to corrosion, A represent atomic weight of iron (56 g), I is corrosion current (amp), t is corrosion duration (s), Z is the valency of reacting electrode (2 for iron), and F is Faraday's constant (96,000 amp s).

4.2. Behavioral Investigations of Corroded Columns

After analyzing effectiveness of accelerated corrosion technique using the above-mentioned parameters, the structural behavior of concrete columns was evaluated for different lengths of concrete column specimens.

5. Specimen Preparation and Instrumentation

For the preparation of the specimens, locally available material was utilized. Ordinary Portland cement, Lawrencepur sand (Lawrencepur Sand Supply Company, Punjab, Pakistan), Marghalla crush (Margalla Crush Stone, Taxila, Pakistan), and potable water were used for the specimen casting. Two different types of concrete mixes were used to achieve a target strength of 21 MPa and 28 MPa. The mix proportions of both mixes are shown in Table 1.

Table 1. Mix Proportion of Concrete.

Sample No.	Cement	Fine Aggregate	Coarse Aggregate	Mix Proportion	Target Strength (MPa)	w/c Ratio
1	1.0	1.74	3.40	1:1.74:3.4	21	0.55
2	1.0	1.75	3.00	1:1.75:3	28	0.47

In general, four types of concrete specimens were cast. Based upon the length of the concrete samples, specimens were designated as R1 to R4. R1 had the least length equal to 300 mm; however, the remaining R2, R3, and R4 specimens had lengths as 500 mm, 700 mm, and 900 mm, respectively. Each group of samples was further divided into two subgroups, named corroded samples and control specimens. Control specimens were designated as "C"; however, the concrete specimens that were gone through the process of accelerated corrosion of embedded reinforcement were designated with the duration of corrosion. The nomenclature for the cast concrete samples is shown in Figure 2.

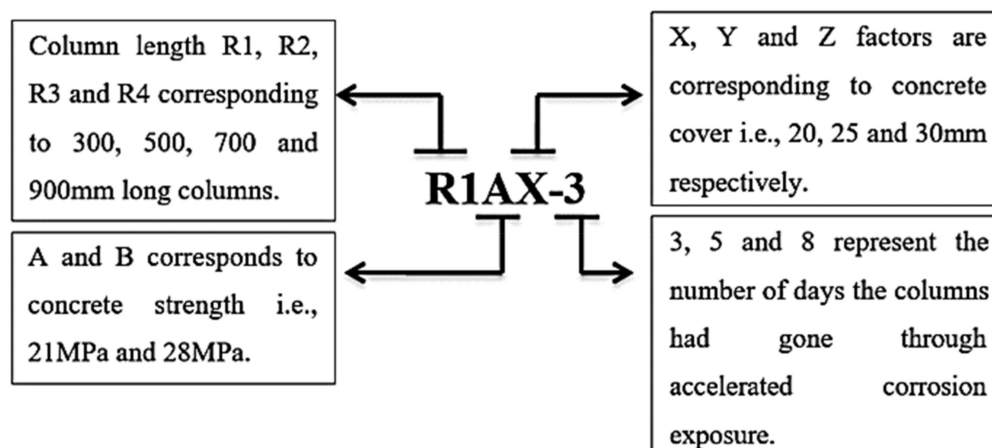


Figure 2. Nomenclature for columns specimen.

In this study, a total of 90 different specimens were cast. The details of these specimens are provided in Table 2. The specimens were reinforced with 4 numbers of 10 mm diameters rebars as longitudinal bar at each corner and lateral stirrups of 10 mm dia. Bar at 100 mm center-to-center as shown in Figure 3. It can be understood from the figure that 300 mm specimen had 3 stirrups while 900 mm specimen had 9 stirrups.

Table 2. Test specimens and designations.

Sr. No.	Specimen Type	Specimen Length (mm)	Concrete Strength (MPa)	Strength Designation	Concrete Cover	Cover Designation	Corrosion Exposure (Days)	Specimen Designation	No. of Specimens
1	R1	300	21	A	20	X	-	R1AX-C	3
2	R1	300	21	A	25	Y	-	R1AY-C	3
3	R1	300	21	A	30	Z	-	R1AZ-C	3
4	R1	300	28	B	20	X	-	R1BX-C	3
5	R1	300	28	B	25	Y	-	R1BY-C	3
6	R1	300	28	B	30	Z	-	R1BZ-C	3
7	R1	300	21	A	20	X	3	R1AX-3	3
8	R1	300	21	A	20	X	5	R1AX-5	3
9	R1	300	21	A	20	X	8	R1AX-8	3
10	R1	300	21	A	25	Y	3	R1AY-3	3
11	R1	300	21	A	25	Y	5	R1AY-5	3
12	R1	300	21	A	25	Y	8	R1AY-8	3
13	R1	300	21	A	30	Z	3	R1AZ-3	3
14	R1	300	21	A	30	Z	5	R1AZ-5	3
15	R1	300	21	A	30	Z	8	R1AZ-8	3
16	R1	300	28	B	20	X	3	R1BX-3	3
17	R1	300	28	B	20	X	5	R1BX-5	3
18	R1	300	28	B	20	X	8	R1BX-8	3
19	R1	300	28	B	25	Y	3	R1BY-3	3
20	R1	300	28	B	25	Y	5	R1BY-5	3
21	R1	300	28	B	25	Y	8	R1BY-8	3
22	R1	300	28	B	30	Z	3	R1BZ-3	3
23	R1	300	28	B	30	Z	5	R1BZ-5	3
24	R1	300	28	B	30	Z	8	R1BZ-8	3
25	R2	500	21	A	25	Y	5	R2AY-5	3
26	R3	700	21	A	25	Y	5	R3AY-5	3
27	R4	900	21	A	25	Y	5	R4AY-5	3
28	R2	500	21	A	25	Y	-	R2AY-C	3
29	R3	700	21	A	25	Y	-	R3AY-C	3
30	R4	900	21	A	25	Y	-	R4AY-C	3

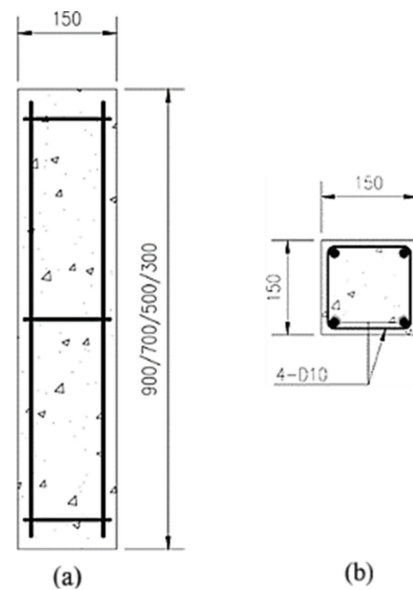


Figure 3. Specimen dimensions (a) Elevation view (b) Cross section view.

5.1. Reinforcement Caging, Electrical Wiring and Concrete Casting

To facilitate the current flow through concrete specimens, before casting samples, electrical connection was made with the reinforcement cage. Electrical wire was connected to one of the bar among reinforcement cage and brought out of the specimen mold to connect with DC source supply. Remaining bars were connected with each other by winding a copper wire on their surface, as shown in Figure 4a,b. The concrete ingredients were weighed separately, as per the ratio of concrete mix, and were added to the concrete mixer. After preparing concrete, it was poured into the molds which were then placed over the shake table and were vibrated for 30 s to release entrapped air within concrete pores. The cast specimens are shown in Figure 4c.

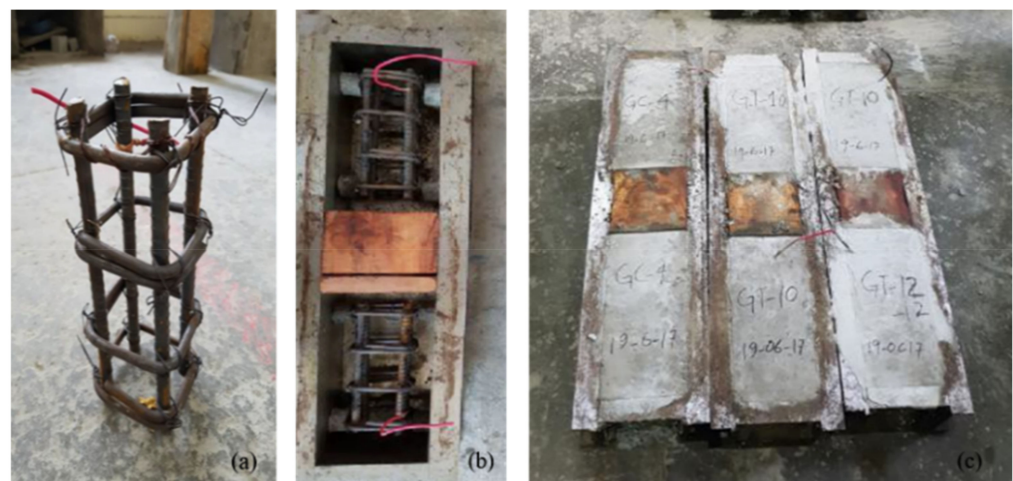


Figure 4. (a) Reinforcement cage with electrical wires. (b) Casting molds. (c) Casted specimens.

5.2. Instrumentation and Accelerated Corrosion Setup

After casting, the column specimens were cured for 28 days, and they were then passed through the process of accelerated corrosion. A constant current was passed through the specimens. In parametric studies, the current was applied to the column specimens for 3, 5, and 8 days. It is important to note that current supply time is an important parameter to obtain constant corrosion in all specimens. For this reason, an hour counter was introduced into the DC source supply. The purpose of the hour counter was to measure the number of

hours through which the circuit was alive. In case of any power failure, the hour counter would stop automatically and on recovery of power supply, hour counter started from the same reading as it was. Output knob consist of anode and cathode, anode was attached to the wire coming from the concrete specimens while cathode was attached to copper strips.

Columns samples were placed in a solution which contain 3.5% NaCl as electrolyte as shown in Figure 5a. NaCl contents of 3.5% resembles the concentration of chloride ions in marine environment. Electrical wires were connected to the reinforcement cage which worked as anode and copper strips present in electrolyte behaved as cathode as shown in Figure 5b. After applying current for specified time of 3, 5 and 8 days, the specimens were removed from circuit.

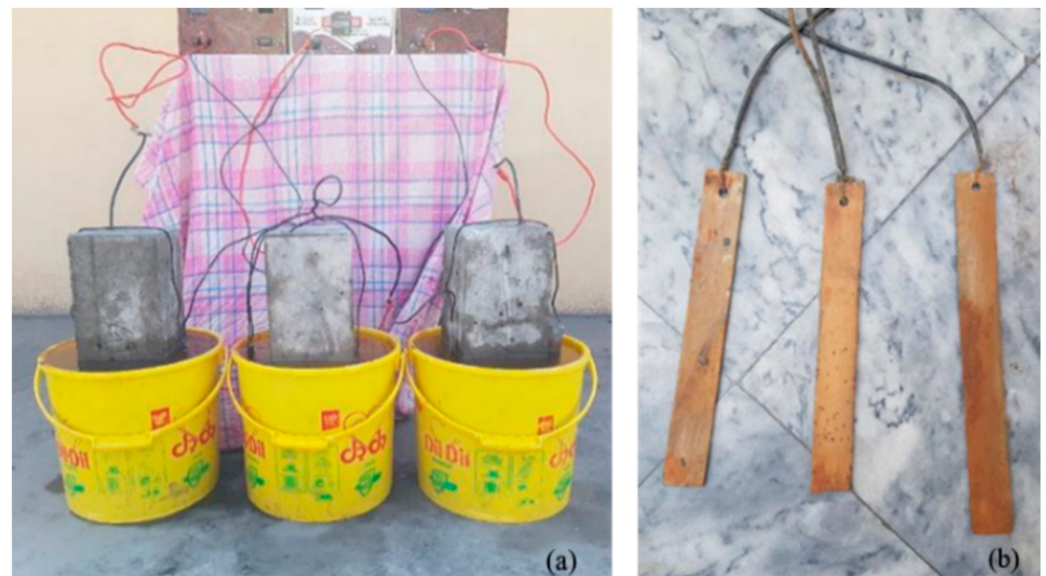


Figure 5. (a) Accelerated corrosion setup. (b) Copper strips (cathode).

6. Testing Results and Discussions

6.1. Specimen Observations

On completion of accelerated corrosion process for specified time, the specimens were removed from the corrosion process. Specimens were inspected against the effect of corrosion on column specimens. The following two major effects of corrosion were observed after accelerated corrosion of concrete columns.

6.1.1. Surface Cracking

The corrosion products occupy almost 6 times more space than the iron particles. These corrosion products exert pressure on the surrounding concrete. Due to this pressure, cracking develops within and on concrete surface. Same phenomena were observed after the accelerated corrosion of column specimens. The corrosion in the column specimens produced diagonal and horizontal cracks due to the corrosion of different rebars, as shown in Figure 6. The diagonal cracks were produced due to the corrosion of longitudinal reinforcement while horizontal cracks produced due to the corrosion of shear ties.

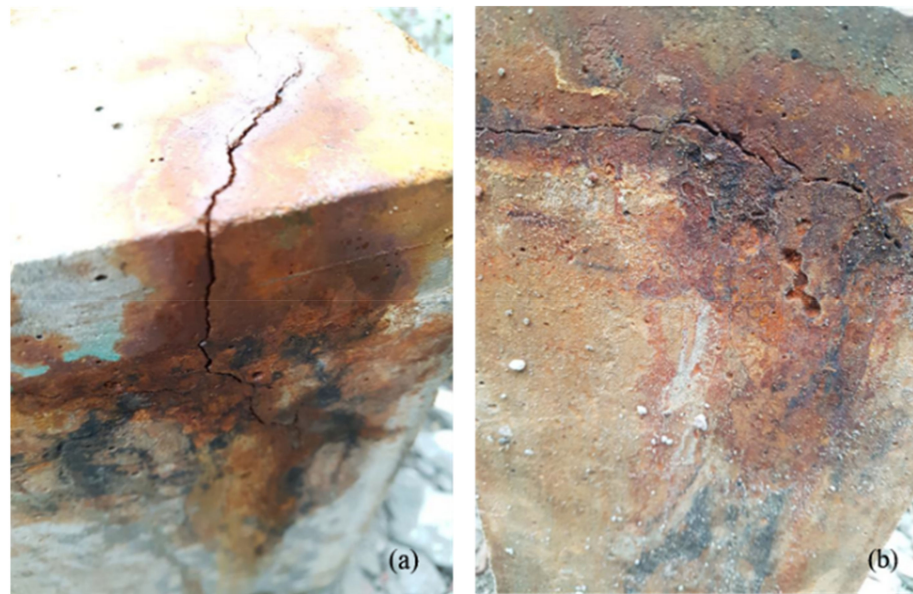


Figure 6. (a) Longitudinal cracking on concrete surface. (b) Horizontal cracking on concrete surface.

6.1.2. Surface Pitting

Concrete surface pitting refers to the formation of small cavities or depressions on the surface of the concrete. This phenomenon can occur due to various factors, including physical damage, chemical attack, or exposure to harsh environmental conditions, which can cause the concrete surface to break down. Concrete surface pitting can accelerate the corrosion process by increasing the surface area of the steel that is exposed to the corrosive environment and it also facilitates a pathway for chloride ions to reach the reinforcement. Poor quality of the concrete can contribute to concrete surface pitting, and the porosity within the concrete affects the rate of chloride ion penetration into the reinforcement. Initially, the concrete specimens resist the flow of chloride contents, making it difficult for current to flow. However, as the corrosion progresses and the ingress of chloride ions reaches the reinforcement, it leads to an increase in the corrosion rate over time, as shown in Figure 7. Therefore, the presence of surface pitting and the level of porosity within the concrete surface affect the rate of chloride ingress, which, in turn, can impact the rate of corrosion.



Figure 7. (a) Surface pitting on column specimen after 5 days. (b) Surface pitting on column specimen after 8 days.

6.2. Axial Compression Testing

On the completion of corrosion process, the specimens were removed from the NaCl solution and were placed in the open environment to dry. After drying, an axial test was performed on the concrete columns. Axial load was applied with the help of 200 ton axial compression machine in laboratory. Before placing the specimens for axial compression test, all type of rust products were removed from the column specimens and loading edges were made plain to distribute load uniformly on the entire surface of the concrete column and produce homogenous results. Corroded and control specimens were loaded up till failure, as shown in Figure 8.



Figure 8. (a) Compression test 300 mm specimen. (b) Compression test 700 mm specimen.

In parametric studies, the column length was taken as 300 mm. In the second phase, columns specimens with varying lengths were tested. In the second phase of study, parameters such as concrete strength, corrosion exposure and concrete cover were taken as constant. Concrete cover was taken as 25 mm; however, corrosion exposure was selected as 5 days. The concrete strength selected for second phase of study was 21 MPa after using the results from parametric studies.

6.3. Effect of Concrete Cover to Axial Load Carrying Capacity

The effect of concrete cover on the axial load carrying capacity of all columns was evaluated and the important results are discussed below.

6.3.1. 21 MPa Specimens

The ultimate load values for the 21 MPa column specimens with 20 mm, 25 mm, and 30 mm concrete covers are shown in Table 3. The results show a gradual decrease in the ultimate load bearing capacity as the corrosion exposure increased from 3 days to 8 days. This shows that the continuous application of accelerated corrosion caused more corrosion products to form, which produce cracking on concrete surface, and hence, peeled off the concrete cover. The corrosion products also decreased the embedded reinforcement diameter that decreased the ultimate load carrying capacity of concrete columns, as can be observed in Figure 9. The data show a similar trend for 25 mm and 30 mm concrete cover, with a slight increase in the ultimate load capacity of column specimens. This shows that the resistance to corrosion increased as the concrete cover increased.

Table 3. Ultimate capacity for 21 MPa concrete column specimens.

Specimen Designation	Concrete Strength (MPa)	Concrete Cover (mm)	Corrosion Exposure (days)	Ultimate Strength (KN)
R1AX-3	21	20	3	539.55
R1AX-3	21	20	3	529.74
R1AX-3	21	20	3	535.36
R1AX-5	21	20	5	519.93
R1AX-5	21	20	5	519.93
R1AX-5	21	20	5	500.31
R1AX-8	21	20	8	490.5
R1AX-8	21	20	8	488.69
R1AX-8	21	20	8	495.405
R1AX-C	21	20	Control	607.46
R1AX-C	21	20	Control	619.6
R1AY-3	21	25	3	557.36
R1AY-3	21	25	3	561.36
R1AY-3	21	25	3	567.55
R1AY-5	21	25	5	541.93
R1AY-5	21	25	5	532.74
R1AY-5	21	25	5	537.12
R1AY-8	21	25	8	501.34
R1AY-8	21	25	8	495.69
R1AY-8	21	25	8	489.5
R1AY-C	21	25	Control	612.13
R1AY-C	21	25	Control	618.08
R1AZ-3	21	30	3	585.6
R1AZ-3	21	30	3	589.41
R1AZ-3	21	30	3	575.17
R1AZ-5	21	30	5	559.17
R1AZ-5	21	30	5	556.36
R1AZ-5	21	30	5	565.31
R1AZ-8	21	30	8	529.74
R1AZ-8	21	30	8	519.93
R1AZ-8	21	30	8	539.55
R1AZ-C	21	30	Control	620.37
R1AZ-C	21	30	Control	612.7

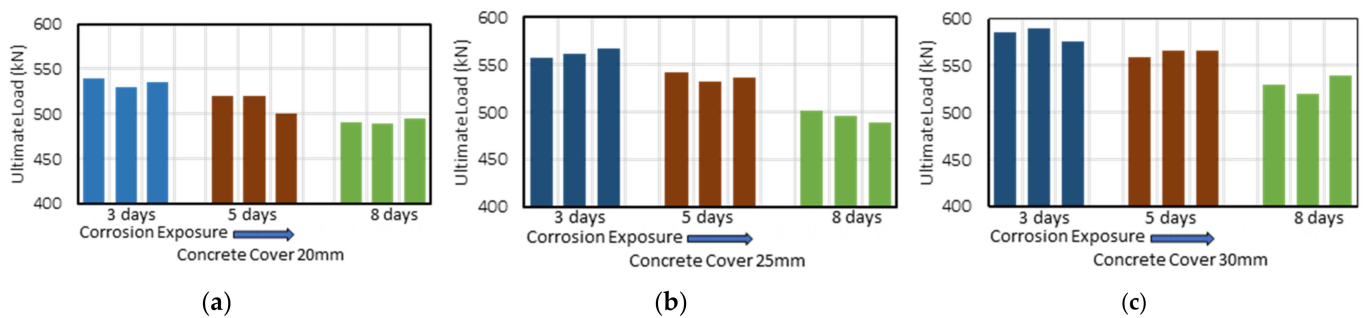


Figure 9. Axial load capacity of column specimens against different exposure levels (a) 20 mm cover (b) 25 mm cover (c) 30 mm cover.

The average values of 3 test specimens for each category of corrosion exposure for specimens having concrete cover 20 mm, 25 mm, and 30 mm is shown in Figure 10. The red line shows the ultimate strength of control specimen. The concrete cover is the primary defense against corrosion initiation in the rebars. A thicker concrete cover offers greater resistance to chloride penetration, making it more difficult for chlorides to reach the rebars and start the corrosion process ultimately providing greater corrosion resistance. As a result, the rebars corrode less and provide better structural integrity for the reinforced

concrete. The result of control samples in Table 3 also indicates that with the increase concrete cover, the ultimate axial load capacity value moves toward the un-corroded control specimens. The percentage difference from the control specimens show much less difference in case of corrosion exposure of 3 days. This represents the fact that the extended corrosive environment causes the reduction in axial load capacity of concrete columns.

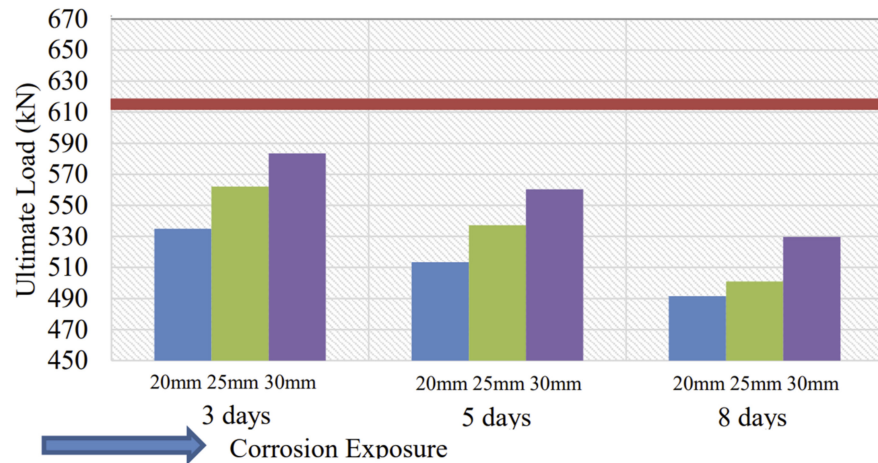


Figure 10. Ultimate axial load capacity vs. exposure level of specimens and concrete cover.

6.3.2. 28 MPa Specimens

The ultimate load values for the 28 Mpa column specimens with 20 mm, 25 mm, and 30 mm concrete cover are shown in Table 4. Figure 11 shows the plot of ultimate strength of these specimens. The results showed a similar trend to 21 MPa specimens. With the increase in corrosion exposure, the load carrying capacity decreased.

Table 4. Ultimate capacity for 28 MPa concrete column specimens.

Specimen Designation	Concrete Strength (MPa)	Concrete Cover (mm)	Corrosion Exposure (Days)	Ultimate Strength (KN)
R1BX-3	28	20	3	562.79
R1BX-3	28	20	3	568.98
R1BX-3	28	20	3	549.36
R1BX-5	28	20	5	529.74
R1BX-5	28	20	5	535.12
R1BX-5	28	20	5	519.93
R1BX-8	28	20	8	500.31
R1BX-8	28	20	8	507.93
R1BX-8	28	20	8	500.31
R1BX-C	28	20	Control	641.04
R1BX-C	28	20	Control	655.52
R1BY-3	28	25	3	583.17
R1BY-3	28	25	3	588.6
R1BY-3	28	25	3	581.17
R1BY-5	28	25	5	549.36
R1BY-5	28	25	5	545.93
R1BY-5	28	25	5	539.55
R1BY-8	28	25	8	510.12
R1BY-8	28	25	8	507.31
R1BY-8	28	25	8	498.5
R1BY-C	28	25	Control	647.55
R1BY-C	28	25	Control	657.55
R1BZ-3	28	30	3	620.08
R1BZ-3	28	30	3	612.32
R1BZ-3	28	30	3	629.7
R1BZ-5	28	30	5	595.27
R1BZ-5	28	30	5	607.7
R1BZ-5	28	30	5	599.65
R1BZ-8	28	30	8	559.17
R1BZ-8	28	30	8	568.6
R1BZ-8	28	30	8	561.22
R1BZ-C	28	30	Control	658.93
R1BZ-C	28	30	Control	643.94

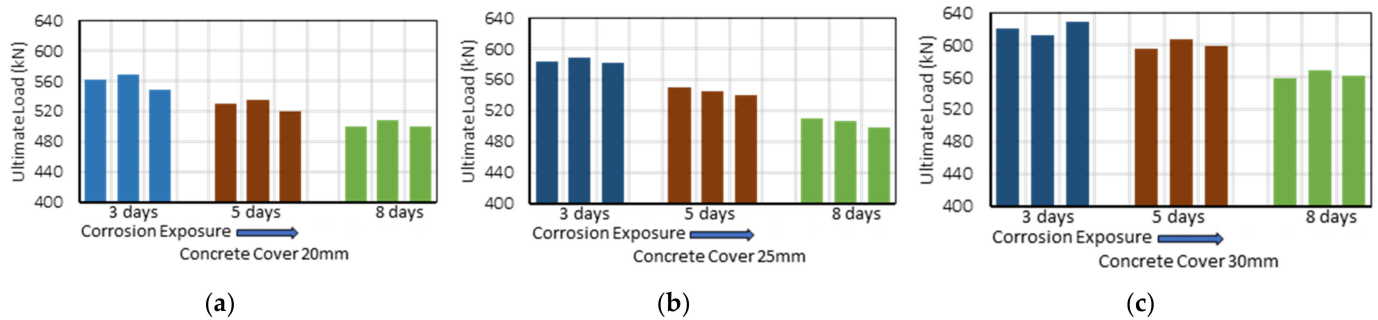


Figure 11. Axial load capacity of column specimens against different exposure levels. (a) 20 mm cover; (b) 25 mm cover; (c) 30 mm cover.

The average values of 3 test specimens for each category of corrosion exposure having concrete cover 20 mm, 25 mm, and 30 mm is shown in Figure 12. The red line shows the ultimate strength of control specimen. Overall, the axial load capacity trend for concrete specimens on longer corrosion exposure decreased. This can be simply explained as the diminishing of oxide layer around the embedded reinforcement that protects steel against corrosion. The resistance of this layer continuously decreased as the corrosion process continued for a longer duration. It also indicates that as we move to higher concrete cover of the column specimens, the load carrying capacity approaches towards the control value. The percentage difference from the control values for the specimens with higher cover is comparatively less than the column specimens having less concrete cover. When we see the effect of corrosion exposure to the concrete column, it can be concluded that corrosion exposure for longer time reduces the axial load capacity considerably by almost 20%. It was also observed that almost 50% axial load capacity reduction only occurred at the initial stage of corrosion. Hence, once the corrosion started, with each passing day, resistance to corrosion started to diminish.

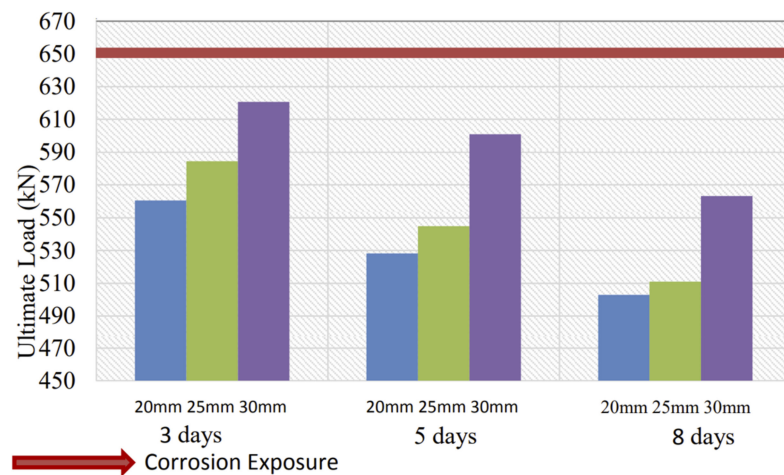


Figure 12. Ultimate axial load capacity vs. exposure level of specimens.

6.4. Reinforcement Weight Loss

The effect of reinforcement weight loss was calculated for both types of concrete and is explained below.

6.4.1. 21 MPa Specimens

The metal loss during the accelerated corrosion process was calculated based upon the weight of reinforcement before and after accelerated corrosion process. The weight of the embedded reinforcement was taken before casting. Once the specimens were tested and cracked, embedded reinforcement in column specimens was extracted and weighted to

determine the loss of metal during the process of accelerated corrosion. Table 5 represents the values of weight of reinforcement prior and after the accelerated corrosion process.

Table 5. Expected vs. actual weight loss of reinforcement for 21 MPa.

Concrete Strength (MPa)	Concrete Cover (mm)	Corrosion Exposure (days)	Expected Weight Loss (Faraday's Law) (g)	Weight before Corrosion (g)	Weight after Corrosion (g)	Percentage Loss (%)
21	20	3	6.38	1500	1417	5.53
21	20	3	6.38	1505	1421	5.58
21	20	3	6.38	1486	1405	5.45
21	20	5	10.64	1565	1421	9.20
21	20	5	10.64	1550	1410	9.03
21	20	5	10.64	1567	1428	8.87
21	20	8	17.02	1499	1267	15.48
21	20	8	17.02	1540	1307	15.13
21	20	8	17.02	1476	1250	15.31
21	25	3	6.54	1475	1411	4.34
21	25	3	6.54	1480	1409	4.80
21	25	3	6.54	1584	1509	4.73
21	25	5	10.91	1603	1470	8.30
21	25	5	10.91	1690	1541	8.82
21	25	5	10.91	1590	1453	8.62
21	25	8	17.45	1601	1363	14.87
21	25	8	17.45	1569	1342	14.47
21	25	8	17.45	1589	1352	14.92
21	30	3	6.71	1315	1279	2.74
21	30	3	6.71	1407	1354	3.77
21	30	3	6.71	1479	1421	3.92
21	30	5	11.18	1414	1302	7.92
21	30	5	11.18	1561	1435	8.07
21	30	5	11.18	1344	1238	7.89
21	30	8	17.89	1483	1284	13.42
21	30	8	17.89	1408	1218	13.49
21	30	8	17.89	1463	1265	13.53

The expected vs. actual weight loss for 21 MPa concrete is plotted in Figure 13. The horizontal lines represent the theoretical weight loss which was expected during the application of direct current. These values are based upon the formulation by Faraday's law. The vertical bars in Figure 13 show the actual percentage loss of rebars that occurred during the accelerated corrosion technique. The reason behind the difference between expected and actual weight loss was due to the resistance provided by the concrete which required a definite amount of current to start the corrosion process, as also explained by Azad et al. [26].

Figure 14 shows the percentage weight loss and axial load-carrying capacity for the concrete strength of 21 MPa. The determination of such a parameter is very important to predict the residual strength of concrete columns against known weight loss.

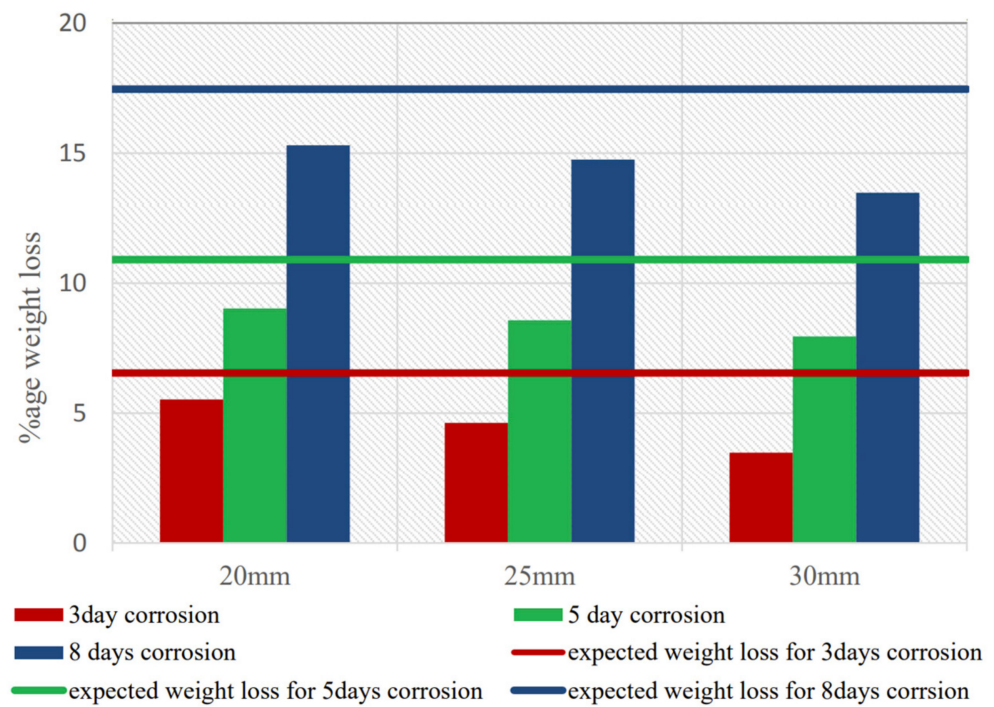


Figure 13. Expected vs. actual weight loss for concrete strength of 21 MPa.

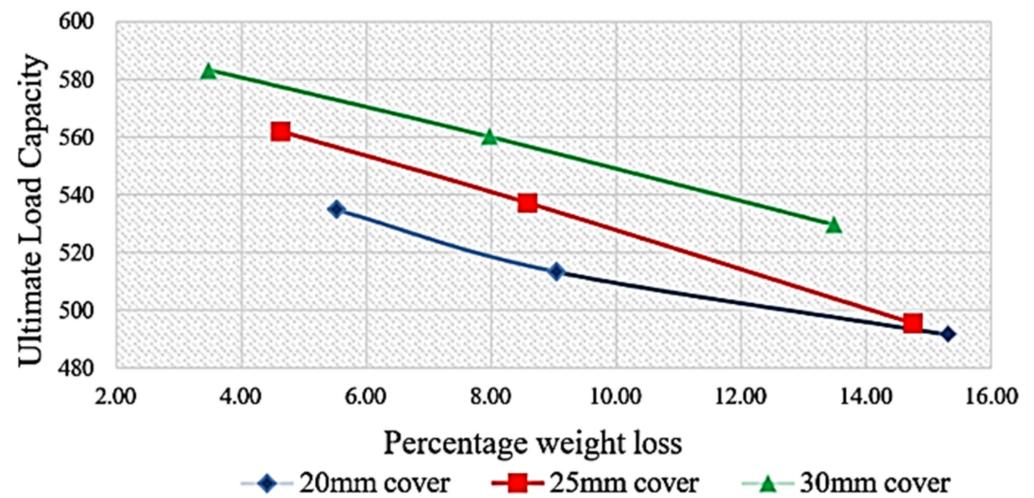


Figure 14. Percentage weight loss vs. ultimate Axial load capacity, for 21 MPa concrete.

6.4.2. 28 MPa Specimens

The actual and expected metal loss for the 28 MPa concrete columns is shown in Table 6. The difference of the percentage of mass loss for higher concrete strength was higher due to the more resistance offered to the applied current to de-pacify the oxidized layer around the embedded reinforcement, as shown in Figure 15. Furthermore, the percentage weight loss and axial load-carrying capacity for 28 MPa concrete columns is shown in Figure 16. A rapid decrease in the load carrying capacity was observed; hence, with such representation one can access the remaining axial load capacity of corroded columns.

Table 6. Expected vs. actual weight loss of reinforcement for 28 MPa.

Concrete Strength (MPa)	Concrete Cover (mm)	Corrosion Exposure (days)	Expected Weight Loss (Faraday’s Law) (g)	Weight before Corrosion (g)	Weight after Corrosion (g)	Percentage (%)
28	20	3	6.38	1460	1389	4.86
28	20	3	6.38	1546	1468	5.05
28	20	3	6.38	1391	1323	4.89
28	20	5	10.64	1484	1354	8.76
28	20	5	10.64	1402	1281	8.63
28	20	5	10.64	1559	1427	8.47
28	20	8	17.02	1534	1301	15.19
28	20	8	17.02	1475	1253	15.05
28	20	8	17.02	1495	1276	14.65
28	25	3	6.54	1544	1481	4.08
28	25	3	6.54	1404	1345	4.20
28	25	3	6.54	1532	1474	3.79
28	25	5	10.91	1574	1449	7.94
28	25	5	10.91	1560	1443	7.50
28	25	5	10.91	1381	1267	8.25
28	25	8	17.45	1465	1259	14.06
28	25	8	17.45	1493	1284	14.00
28	25	8	17.45	1570	1329	15.35
28	30	3	6.71	1432	1396	2.51
28	30	3	6.71	1496	1451	3.01
28	30	3	6.71	1404	1361	3.06
28	30	5	11.18	1578	1473	6.65
28	30	5	11.18	1603	1501	6.36
28	30	5	11.18	1548	1439	7.04
28	30	8	17.89	1533	1334	12.98
28	30	8	17.89	1569	1379	12.11
28	30	8	17.89	1552	1349	13.08

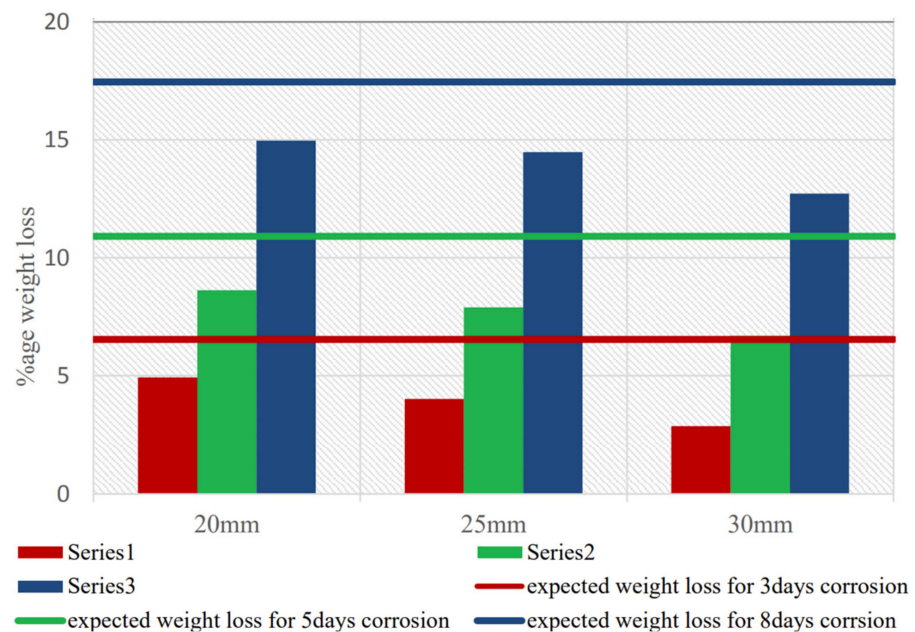


Figure 15. Expected vs. actual weight loss for concrete strength of 28 MPa.

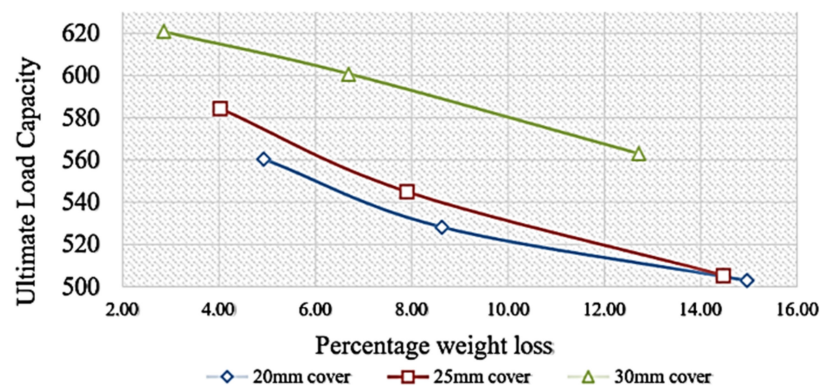


Figure 16. Percentage weight loss vs. ultimate Axial load capacity, for 28 MPa concrete.

6.5. Effect of Corroded Column Length on Axial Load Capacity

The effect of corrosion on axial strength of column was also investigated for 21 MPa concrete strength specimens with 25 mm concrete cover and with varying lengths of columns including 500 mm, 700 mm, and 900 mm. The specimens were applied to the process of accelerated corrosion for the duration of 5 days. Although increasing length of column reduces the ultimate load carrying as per Euler buckling formula, the focus of this study was the effect of corrosion on columns. The tabular results of percentage in weight loss are shown in Table 7. The ultimate load capacity of different columns is shown in Figure 17, where the red arrows show the direction along the axis in which the column length is increasing. The compression load capacity decreased with increase in the length of column. The same trend can be seen in the control specimens axial load capacities, i.e., column with least height shows higher axial load capacity, and column having greater lengths shows the lower load capacity. A visible reduction in test samples and control samples can be seen. However, the difference between axial load capacities of control and corroded concrete columns for smaller length of column was less compared to the column with longer length. The reason behind this phenomenon was the combined effect of corrosion of longitudinal reinforcement and lateral ties. Corrosion of longitudinal reinforcement produces corrosion products that exert higher pressure on surrounding concrete and result in loss of concrete cover. Secondly, the corrosion of ties reduces the cross-sectional area of the ties and reduces confinement of concrete. This is why concrete columns having greater length of columns exhibit more loss in load carrying capacity due to no or very less confinement and reduction in reinforcement steel diameter. An important thing to be noted here is that for the column with length of 900 mm, the percentage weight loss of metal was just about 2.5%. The value of steel loss did not make a significant impact on the reduction in steel diameter. This is why we can conclude that the load-carrying capacity of column not only depends upon the reduction in reinforcement, but it also depends upon the spalling of concrete and loss of bond between concrete and steel.

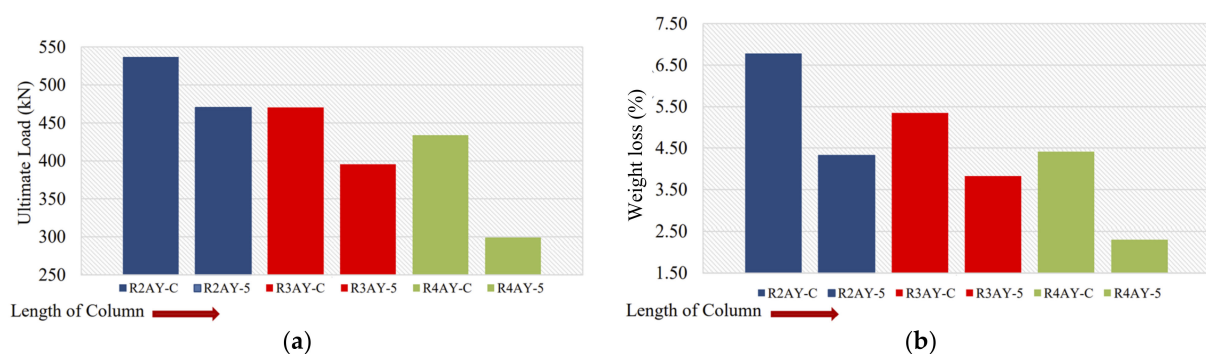


Figure 17. (a) Ultimate load capacity vs. corroded length of columns; (b) expected vs. actual weight loss for different corroded lengths.

Table 7. Effect of corroded length of column on axial strength of column.

Specimen Length (mm)	Sample Designation	Ultimate Load (KN)	Expected Weight Loss (Faraday's Law) (g)	Weight before Corrosion (g)	Weight after Corrosion (g)	Percentage (%)
500	R2AY-5	492.462	6.78	1700	1631	4.06
500	R2AY-51	476.766	6.78	1675	1605	4.18
500	R2AY-52	441.45	6.78	1567	1493	4.72
500	R2AY-C	525.816	NA	NA	NA	NA
500	R2AY-C	547.398	NA	NA	NA	NA
700	R3AY-5	397.305	5.35	2150	2067	3.86
700	R3AY-5	406.134	5.35	2100	2021	3.76
700	R3AY-5	381.609	5.35	1800	1731	3.83
700	R3AY-C	458.127	NA	NA	NA	NA
700	R3AY-C	482.652	NA	NA	NA	NA
900	R4AY-5	290.376	4.42	2500	2443	2.28
900	R4AY-5	327.654	4.42	2375	2313	2.61
900	R4AY-5	279.585	4.42	2333	2286	2.01
900	R4AY-C	410.058	NA	NA	NA	NA
900	R4AY-C	457.146	NA	NA	NA	NA

7. Conclusions

Based upon the experimental results as discussed above, the following conclusions can be drawn.

- The concrete cover serves as the initial line of defense against corrosion of the reinforcement. A thicker concrete cover provides greater resistance against corrosion. The results demonstrated a 10% difference in percentage between column specimens with a cover of 30 mm and those with a cover of 20 mm.
- The column specimens that encounter corrosive and hostile environment exhibit a 10–20% decrease in axial control capacity. Out of this reduction, a corroded column with less concrete cover experiences a reduction of over 50% during the early stages of corrosion.
- The concrete strength also has a significant effect on the corrosion of specimens. The specimens with higher concrete strength exhibit less surface cracking and surface pitting, resulting in reduced corrosion. The experimental findings identified that when concrete strength was raised by 25%, column specimens' axial capacities increased by 4%.
- The corrosion can have a substantial impact on the axial load capacity of the column specimens when they have small cover combined with reduced reinforcement area and increased length. The experimental results indicated a 25% reduction in the axial capacity when the column height was increased from 700 mm to 900 mm.

Author Contributions: Conceptualization, A.H. and I.A.; formal analysis, A.M.R.; funding acquisition, A.B.M.; investigation, I.A., A.M.R., M.F.U.D.A., A.J. and A.H.; methodology, A.H. and I.A.; supervision, A.H. and A.B.M.; writing—original draft, M.F.U.D.A., A.J. and I.A.; writing—review and editing, A.H., A.M.R., M.U.Q. and A.B.M. All authors have read and agreed to the published version of the manuscript.

Funding: Internally funded by the Civil Engineering Department, University of Engineering and Technology, Lahore 54000, Pakistan.

Institutional Review Board Statement: Not applicable.

Informed Consent Statement: Not applicable.

Data Availability Statement: Not applicable.

Acknowledgments: The authors gratefully acknowledge the Department of Civil Engineering, University of Engineering and Technology, Lahore, Pakistan, for providing research, financial, and experimental facilities. Experts from National Engineering Services Pakistan (NESPAK) are gratefully acknowledged for providing technical assistance. The authors would like to thank Florida International University, Miami, Florida, USA, and Sohar University, Sohar, Oman, for supporting the publication of this manuscript.

Conflicts of Interest: The authors declare no conflict of interest.

References

1. Dixit, M.; Gupta, A.K. A Review of Different Assessment Methods of Corrosion of Steel Reinforcement in Concrete. *Iran. J. Sci. Technol. Trans. Civ. Eng.* **2022**, *46*, 735–752. [CrossRef]
2. Poston, R.W.; West, J.S. Investigation of the Charlotte Motor Speedway Bridge Collapse. In Proceedings of the Structures Congress 2005: Metropolis and Beyond, New York, NY, USA, 20–24 April 2005; pp. 1–11.
3. Hameed, A.; Rasool, A.M.; Ibrahim, Y.E.; Afzal, M.F.U.D.; Qazi, A.U.; Hameed, I. Utilization of Fly Ash as a Viscosity-Modifying Agent to Produce Cost-Effective, Self-Compacting Concrete: A Sustainable Solution. *Sustainability* **2022**, *14*, 11559. [CrossRef]
4. Ortiz, J.D.; Dolati, S.S.K.; Malla, P.; Nanni, A.; Mehrabi, A. FRP-Reinforced/Strengthened Concrete: State-of-the-Art Review on Durability and Mechanical Effects. *Materials* **2023**, *16*, 1990. [CrossRef] [PubMed]
5. Khodayari, A.; Mantawy, I.M.; Azizinamini, A. Experimental and Numerical Investigation of Prefabricated Concrete Barrier Systems Using Ultra-High-Performance Concrete. *Transp. Res. Rec. J. Transp. Res. Board* **2023**, 036119812311625. [CrossRef]
6. Saingam, P.; Ejaz, A.; Ali, N.; Nawaz, A.; Hussain, Q.; Joyklad, P. Prediction of Stress–Strain Curves for HFRP Composite Confined Brick Aggregate Concrete under Axial Load. *Polymers* **2023**, *15*, 844. [CrossRef]
7. Malla, P.; Dolati, S.S.K.; Ortiz, J.D.; Mehrabi, A.B.; Nanni, A.; Dinh, K. Feasibility of Conventional Non-Destructive Testing Methods in Detecting Embedded FRP Reinforcements. *Appl. Sci.* **2023**, *13*, 4399. [CrossRef]
8. Ebell, G.; Burkert, A.; Fischer, J.; Lehmann, J.; Müller, T.; Meinel, D.; Paetsch, O. Investigation of chloride-induced pitting corrosion of steel in concrete with innovative methods. *Mater. Corros.* **2016**, *67*, 583–590. [CrossRef]
9. Javed, A.; Krishna, C.; Ali, K.; Afzal, M.F.U.D.; Mehrabi, A.; Meguro, K. Micro-Scale Experimental Approach for the Seismic Performance Evaluation of RC Frames with Improper Lap Splices. *Infrastructures* **2023**, *8*, 56. [CrossRef]
10. Ejaz, A.; Ruangrassamee, A.; Kruavit, P.; Udomworarat, P.; Wijeyewickrema, A.C. Strengthening of substandard lap splices using hollow steel section (HSS) collars. *Structures* **2022**, *46*, 128–145. [CrossRef]
11. Basit, S.; Maki, T.; Mutsuyoshi, H.; Ishihara, Y.; Tajima, H. Influence of reinforcement arrangement details on mechanical behavior of precast concrete barrier with loop connection. *Structures* **2020**, *27*, 1682–1692. [CrossRef]
12. Afzal, M.F.U.D.; Matsumoto, Y.; Nohmi, H.; Sakai, S.; Su, D.; Nagayama, T. Comparison of Radar Based Displacement Measurement Systems with Conventional Systems in Vibration Measurements at a Cable Stayed Bridge. In Proceedings of the 11th German-Japan Bridge Symposium, Osaka, Japan, 30–31 August 2016. Available online: <https://www.researchgate.net/publication/307932143> (accessed on 26 April 2023).
13. Awan, M.S.; Javed, A.; Afzal, M.F.U.D.; Vilchez, L.F.N.; Mehrabi, A. Evaluation of System Identification Methods for Free Vibration Flutter Derivatives of Long-Span Bridges. *Appl. Sci.* **2023**, *13*, 4672. [CrossRef]
14. Mustafa, A.E.; Javed, A.; Ali, K. Safety Assessment of Cables of Suspension Bridge under Blast Load. In Proceedings of the Structures Congress 2022, Atlanta, GA, USA, 20–23 April 2022; pp. 79–93. [CrossRef]
15. Ali, K.; Javed, A.; Mustafa, A.E.; Saleem, A. Blast-Loading Effects on Structural Redundancy of Long-Span Suspension Bridge Using a Simplified Approach. *Pract. Period. Struct. Des. Constr.* **2022**, *27*, 04022024. [CrossRef]
16. Ashraf, S.; Ali, M.; Shrestha, S.; Hafeez, M.A.; Moiz, A.; Sheikh, Z.A. Impacts of climate and land-use change on groundwater recharge in the semi-arid lower Ravi River basin, Pakistan. *Groundw. Sustain. Dev.* **2022**, *17*, 100743. [CrossRef]
17. Javed, A.; Sadeghnejad, A.; Yakel, A.; Azizinamini, A. Magnetic Flux Leakage (MFL) Method for Damage Detection in Internal Post-Tensioning Tendons. 2021. Available online: <https://rosap.nrl.bts.gov/view/dot/62244> (accessed on 27 April 2023).
18. Javed, A.; Mantawy, I.M.; Azizinamini, A. 3D-Printing of Ultra-High-Performance Concrete for Robotic Bridge Construction. *Transp. Res. Rec. J. Transp. Res. Board* **2021**, 2675, 307–319. [CrossRef]
19. Lu, Y.-Y.; Hu, J.-Y.; Li, S.; Tang, W.-S. Active and passive protection of steel reinforcement in concrete column using carbon fibre reinforced polymer against corrosion. *Electrochim. Acta* **2018**, *278*, 124–136. [CrossRef]
20. Meda, A.; Mostosi, S.; Rinaldi, Z.; Riva, P. Experimental evaluation of the corrosion influence on the cyclic behaviour of RC columns. *Eng. Struct.* **2014**, *76*, 112–123. [CrossRef]
21. Xu, J.-G.; Cai, Z.-K.; Feng, D.-C. Life-cycle seismic performance assessment of aging RC bridges considering multi-failure modes of bridge columns. *Eng. Struct.* **2021**, *244*, 112818. [CrossRef]
22. Ma, Y.; Che, Y.; Gong, J. Behavior of corrosion damaged circular reinforced concrete columns under cyclic loading. *Constr. Build. Mater.* **2012**, *29*, 548–556. [CrossRef]
23. Xu, J.-G.; Feng, D.-C.; Wu, G.; Cotsovov, D.M.; Lu, Y. Analytical modeling of corroded RC columns considering flexure-shear interaction for seismic performance assessment. *Bull. Earthq. Eng.* **2019**, *18*, 2165–2190. [CrossRef]

24. Misra, S.; Uomoto, T. Behavior of Concrete Beams and Columns in Marine Environment When Corrosion of Reinforcing Bars Takes Place. *Spec. Publ.* **1988**, *109*, 127–146.
25. Rodriguez, J.; Ortega, L.M.; Casal, J.; Arenas, D.J.M. Load Bearing Capacity of Concrete Columns with Corroded Reinforcement. In Proceedings of the Fourth International Symposium, Cambridge, UK, 1–4 July 1996.
26. Azad, A.K.; Al-Osta, M.A. Capacity of Corrosion-Damaged Eccentrically Loaded Reinforced Concrete Columns. *ACI Mater. J.* **2014**, *111*, 711–722. [[CrossRef](#)]
27. Broomfield, J.G. *Corrosion of Steel in Concrete: Understanding, Repair and Investigation*; CRC Press: Boca Raton, FL, USA, 1997.
28. Yuvaraj, S.; Nirmalkumar, K.; Kumar, V.R.; Gayathri, R.; Mukilan, K.; Shubiksha, S. Influence of corrosion inhibitors in reinforced concrete—A state of art of review. *Mater. Today Proc.* **2022**, *68*, 2406–2412. [[CrossRef](#)]
29. Liu, Y.; Hao, H.; Hao, Y. Blast fragility analysis of RC columns considering chloride-induced corrosion of steel reinforcement. *Struct. Saf.* **2022**, *96*, 102200. [[CrossRef](#)]
30. Zhou, Y.; Gencturk, B.; Willam, K.; Attar, A. Carbonation-Induced and Chloride-Induced Corrosion in Reinforced Concrete Structures. *J. Mater. Civ. Eng.* **2015**, *27*, 04014245. [[CrossRef](#)]
31. Vu, N.S.; Yu, B.; Li, B. Prediction of strength and drift capacity of corroded reinforced concrete columns. *Constr. Build. Mater.* **2016**, *115*, 304–318. [[CrossRef](#)]
32. Soltani, A.; Nasserasadi, K.; Ahmadi, J.; Tafakori, E. Empirical assessment and refinement of corrosion distribution models in the perimeter of corroded steel rebar subjected to chloride ions attack. *Case Stud. Constr. Mater.* **2022**, *17*, e01398. [[CrossRef](#)]
33. Han, L.-H.; Hou, C.-C.; Wang, Q.-L. Behavior of circular CFST stub columns under sustained load and chloride corrosion. *J. Constr. Steel Res.* **2014**, *103*, 23–36. [[CrossRef](#)]
34. Alonso, C.; Andrade, C.; Rodriguez, J.; Diez, J.M. Factors controlling cracking of concrete affected by reinforcement corrosion. *Mater. Struct.* **1998**, *31*, 435–441. [[CrossRef](#)]
35. Chernin, L.; Val, D.V.; Volokh, K.Y. Analytical modelling of concrete cover cracking caused by corrosion of reinforcement. *Mater. Struct.* **2009**, *43*, 543–556. [[CrossRef](#)]
36. Guzmán, S.; Gálvez, J.C.; Sancho, J.M. Cover cracking of reinforced concrete due to rebar corrosion induced by chloride penetration. *Cem. Concr. Res.* **2011**, *41*, 893–902. [[CrossRef](#)]
37. Bossio, A.; Monetta, T.; Bellucci, F.; Lignola, G.P.; Prota, A. Modeling of concrete cracking due to corrosion process of reinforcement bars. *Cem. Concr. Res.* **2015**, *71*, 78–92. [[CrossRef](#)]
38. Cabrera, J. Deterioration of Concrete Due to Reinforcement Steel Corrosion. *Cem. Concr. Compos.* **1996**, *18*, 47–59. [[CrossRef](#)]
39. Choi, Y.S.; Yi, S.-T.; Kim, M.Y.; Jung, W.Y.; Yang, E.I. Effect of corrosion method of the reinforcing bar on bond characteristics in reinforced concrete specimens. *Constr. Build. Mater.* **2014**, *54*, 180–189. [[CrossRef](#)]
40. Al-Sulaimani, G.J.; Kaleemullah, M.; Basunbul, I.A.; Rasheeduzzafar. Influence of Corrosion and Cracking on Bond Behavior and Strength of Reinforced Concrete Members. *Struct. J.* **1990**, *87*, 220–231.
41. Ma, Y.; Guo, Z.; Wang, L.; Zhang, J. Experimental investigation of corrosion effect on bond behavior between reinforcing bar and concrete. *Constr. Build. Mater.* **2017**, *152*, 240–249. [[CrossRef](#)]
42. Saifullah, M. Effect of Reinforced Corrosion on Bond Strength in Reinforced Concrete. Doctoral Dissertation, The University of Birmingham, Birmingham, UK, 1994.
43. Fang, C.; Lundgren, K.; Plos, M.; Gylltoft, K. Bond behaviour of corroded reinforcing steel bars in concrete. *Cem. Concr. Res.* **2006**, *36*, 1931–1938. [[CrossRef](#)]
44. Hua, J.; Fan, H.; Xue, X.; Wang, F.; Chen, Z.; Huang, L.; Wang, N. Tensile and low-cycle fatigue performance of bimetallic steel bars with corrosion. *J. Build. Eng.* **2021**, *43*, 103188. [[CrossRef](#)]
45. Hua, J.; Wang, F.; Huang, L.; Wang, N.; Xue, X. Experimental study on mechanical properties of corroded stainless-clad bimetallic steel bars. *Constr. Build. Mater.* **2021**, *287*, 123019. [[CrossRef](#)]
46. Hua, J.; Wang, F.; Wang, N.; Huang, L.; Hai, L.; Li, Y.; Zhu, X.; Xue, X. Experimental and numerical investigations on corroded stainless-clad bimetallic steel bar with artificial damage. *J. Build. Eng.* **2021**, *44*, 102779. [[CrossRef](#)]
47. François, R.; Khan, I.; Dang, V.H. Impact of corrosion on mechanical properties of steel embedded in 27-year-old corroded reinforced concrete beams. *Mater. Struct.* **2012**, *46*, 899–910. [[CrossRef](#)]
48. Apostolopoulos, C.A. The Influence of Corrosion and Cross-Section Diameter on the Mechanical Properties of B500c Steel. *J. Mater. Eng. Perform.* **2008**, *18*, 190–195. [[CrossRef](#)]
49. Arockiasamy, M.; Arvan, P.A. Behavior, Performance, and Evaluation of Prestressed Concrete/Steel Pipe/Steel H-Pile to Pile Cap Connections. *Pract. Period. Struct. Des. Constr.* **2022**, *27*, 03122001. [[CrossRef](#)]
50. Arvan, P.A.; Arockiasamy, M. Energy-Based Approach: Analysis of a Laterally Loaded Pile in Multi-Layered Non-Linear Elastic Soil Strata. *Geotechnics* **2022**, *2*, 570–598. [[CrossRef](#)]
51. Zhang, W.; Chen, J.; Luo, X. Effects of impressed current density on corrosion induced cracking of concrete cover. *Constr. Build. Mater.* **2019**, *204*, 213–223. [[CrossRef](#)]
52. Ha, T.-H.; Muralidharan, S.; Bae, J.-H.; Ha, Y.-C.; Lee, H.-G.; Park, K.-W.; Kim, D.-K. Accelerated short-term techniques to evaluate the corrosion performance of steel in fly ash blended concrete. *Build. Environ.* **2007**, *42*, 78–85. [[CrossRef](#)]
53. Yuan, Y.; Ji, Y.; Shah, S.P. Comparison of two accelerated corrosion techniques for concrete structures. *ACI Struct. J.* **2007**, *104*, 344–347.

54. Husain, A.; Al-Bahar, S.; Salam, S.A.; Al-Shamali, O. Accelerated AC impedance testing for prequalification of marine construction materials. *Desalination* **2004**, *165*, 377–384. [[CrossRef](#)]
55. Geng, C.; Xu, Y.; Weng, D. A new method to quickly assess the inhibitor efficiency. *J. Wuhan Univ. Technol. Sci. Ed.* **2008**, *23*, 950–954. [[CrossRef](#)]
56. YuBun, A.; Balaguru, P.; Chung, L. Bond Behavior of Corroded Reinforcement Bars. *ACI Mater. J.* **2000**, *97*, 214–220.
57. Caré, S.; Raharinaivo, A. Influence of impressed current on the initiation of damage in reinforced mortar due to corrosion of embedded steel. *Cem. Concr. Res.* **2007**, *37*, 1598–1612. [[CrossRef](#)]

Disclaimer/Publisher’s Note: The statements, opinions and data contained in all publications are solely those of the individual author(s) and contributor(s) and not of MDPI and/or the editor(s). MDPI and/or the editor(s) disclaim responsibility for any injury to people or property resulting from any ideas, methods, instructions or products referred to in the content.